Wave-Convection Interactions Amplify Convective Parameterization Biases in the South Pacific Convergence Zone

Yuanrui Chen[1], Wenchao Chu[1], Jonathon S. Wright[1], Yanluan Lin[1]

[1]Department of Earth System Science, Ministry of Education Key Laboratory for Earth System Modeling, Tsinghua University, Beijing, China

Key Points:

- An improved deep convection parameterization reduces biases in the South Pacific Convergence Zone (SPCZ), especially for heavy rainfall.
- Biases in simulated precipitation rate affect diabatic heating and the upper-level response to transient Rossby waves.
- More realistic upper-level heating strengthens feedbacks between waves and convection, blocking propagation of wave energy locally.

Corresponding author: Jonathon S. Wright, `jswright@tsinghua.edu.cn`

Abstract

Climate models have long-standing difficulties simulating the South Pacific Convergence Zone (SPCZ) and its variability. For example, the default Zhang-McFarlane (ZM) convection scheme in the Community Atmosphere Model version 5 (CAM5) produces too much light precipitation and too little heavy precipitation in the SPCZ, with this bias toward light precipitation even more pronounced in the SPCZ than in the tropics as a whole. Here, we show that implementing a recently developed convection scheme in the CAM5 yields significant improvements in the simulated SPCZ during austral summer and discuss the reasons behind these improvements. In addition to intensifying both mean rainfall and its variability in the SPCZ, the new scheme produces a larger heavy rainfall fraction that is more consistent with observations and state-of-the-art reanalyses. This shift toward heavier, more variable rainfall increases both the magnitude and altitude of diabatic heating associated with convective precipitation, intensifying lower tropospheric convergence and increasing the influence of convection on the upper-level circulation. Increased diabatic production of potential vorticity in the upper troposphere intensifies the distortion effect exerted by convection on transient Rossby waves that pass through the SPCZ. Weaker distortion effects in simulations using the ZM scheme allow waves to propagate continuously through the region rather than dissipating locally, further reducing updrafts and weakening convection in the SPCZ. Our results outline a dynamical framework for evaluating model representations of tropical–extratropical interactions within the SPCZ and clarify why convective parameterizations that produce 'top-heavy' profiles of deep convective heating better represent the SPCZ and its variability.

Plain Language Summary

The South Pacific convergence zone (SPCZ), a band of strong rainfall that stretches diagonally across the South Pacific from northwest to southeast, is difficult for climate models to simulate well. Here, we suggest that much of this difficulty stems from underestimating both how much heavy rainfall is produced in the SPCZ and how high above the surface this rainfall forms. The SPCZ has previously been described as a 'graveyard' for weather systems. Our hypothesis casts the SPCZ more as a toll collector and suggests that the vertical location of the collection point is key. Simulated weather systems that produce heavier rainfall as they move through the SPCZ region release energy higher in the atmosphere, providing the SPCZ with the means to maintain itself. A model that releases this energy lower in the atmosphere by producing too much light rain allows many weather systems to bypass the toll, weakening the simulated SPCZ and drawing it equatorward in search of the energy it needs.

1 Introduction

The South Pacific Convergence Zone (SPCZ) is a band of strong rainfall that extends diagonally across the South Pacific, spanning more than 30 degrees of latitude from New Guinea in the northwest to the central South Pacific in the southeast (D. G. Vincent, 1994). Since satellite images provided the first views of large-scale precipitation in the SPCZ in the 1960s (Hubert, 1961), studies of the SPCZ have consistently emphasized the importance of tropical–extratropical interactions in its dynamics, primarily through transient Rossby waves (Kiladis & Weickmann, 1992; Matthews et al., 1996; Widlansky et al., 2010; Matthews, 2012; van der Wiel et al., 2015, 2016b, 2016a). Variations in the intensity and position of rainfall in the SPCZ affect the weather and climate of land areas and islands across the South Pacific (e.g., W. Cai et al., 2012; E. M. Vincent et al., 2011).

Global climate models (GCMs) have long struggled to simulate the orientation and variability of the austral summertime SPCZ (Brown et al., 2011, 2012; Niznik & Lintner, 2013; Niznik et al., 2015; Lintner et al., 2016). For example, the simulated SPCZ in many GCMs is oriented west-to-east, rather than southeastward into the subtropical South Pacific. Multi-model mean slopes based on GCM simulations completed for the Coupled Model Intercomparison Project 5 (CMIP5; Taylor et al., 2012) showed only -0.09 degrees latitude per degree longitude, only about one-third of the slope based on observations (Brown et al., 2012). This zonal orientation renders the SPCZ indistinguishable from a second intertropical convergence zone (ITCZ) in the Southern Hemisphere, leading to the so-called double ITCZ bias (Mechoso et al., 1995; J.-L. Lin, 2007; X. Zhang et al., 2015). Many models also cannot reliably reproduce variability in the SPCZ on synoptic scales, such as feedback with transient waves, or interannual scales, such as the response to El Niño (Niznik et al., 2015; W. Cai et al., 2012; Borlace et al., 2014). Although problems in simulating the SPCZ are linked to errors in sea surface temperatures (SSTs), previous studies have shown that atmospheric models forced by observed SSTs may still struggle to simulate the intensity and variability of the SPCZ (Ashfaq et al., 2010; Niznik & Lintner, 2013; G. Li & Xie, 2014; Niznik et al., 2015; Beischer et al., 2021).

Owing to the diagonal orientation of the SPCZ, precipitation in this region is much more intimately connected to tropical–extratropical interactions than the ITCZ in the Northern Hemisphere. For example, Trenberth (1976) referred to the SPCZ as a 'graveyard' for synoptic fronts from the southwest. Synoptic waves are refracted by local potential vorticity (PV) gradients from the Australian subtropical jet to the upper-tropospheric westerly winds over the equatorial eastern Pacific (van der Wiel et al., 2015), also known as the 'westerly duct' (Hoskins & Ambrizzi, 1993). Anomalous ascent associated with these weather systems passing through the SPCZ can trigger transient bursts of diagonally–oriented deep convection (van der Wiel et al., 2016a; Brown et al., 2020). Negative zonal stretching deformation by the background state ($\partial U/\partial x < 0$) and wave–convection feedback during convective events slow the propagation of transient waves, so that eddy energy tends to 'pulse' in the SPCZ region (Widlansky et al., 2010; Matthews, 2012; van der Wiel et al., 2016a). The blocking effect of the Andes also influences the SPCZ by modulating the dry zone above the subtropical southeastern Pacific, which regulates the lower tropospheric inflow of moisture to the SPCZ (Takahashi & Battisti, 2007; Lintner & Neelin, 2008; Niznik & Lintner, 2013).

Although wave–convection feedback is a critical part of tropical–extratropical interactions in the SPCZ, many models cannot simulate it well (Matthews, 2012; van der Wiel et al., 2015, 2016a; Niznik et al., 2015). Wave-induced convection in the SPCZ triggers upper-level divergence and lower-level convergence that distorts the original Rossby waves in turn, resulting in a negative feedback that acts to dissipate the wave (Matthews, 2012). These secondary circulations, which modulate transient eddies in the upper troposphere, result primarily from strong latent heat release in deep convection (van der Wiel et al., 2016a). van der Wiel et al. (2016a) showed that this distortion effect is fragile when time-varying diabatic heating is replaced by its climatological mean, allowing waves to propagate continuously through the region rather than dissipating locally. The resulting changes in wave behavior generate significant negative precipitation biases, indicating that wave–convection feedback is critical for simulating a realistic SPCZ. Although most of the models contributing to CMIP5 could capture the dynamics of low-level inflow in the SPCZ, these same models showed considerable spread in wave dissipation in the SPCZ region (Niznik & Lintner, 2013; Niznik et al., 2015). These models tended to produce transient waves that propagated too quickly in both coupled and atmosphere-only simulations, suggesting that the models could not adequately reproduce wave deceleration resulting from wave–convection feedback (Niznik et al., 2015; van der Wiel et al., 2016a). Niznik et al. (2015) further showed that northwestward propagation of anomalous precipitation into the tropical part of the SPCZ was reduced in GCM simulations relative to reanalysis products, suggesting weaker interactions between the tropics and extratropics.

Although previous work has shown that the double-ITCZ bias in GCMs is sensitive to the choice of convection schemes (G. J. Zhang & Wang, 2006; G. J. Zhang & Song, 2010; Hirota et al., 2011; Oueslati & Bellon, 2013; Song & Zhang, 2018), few studies have examined the role of convective parameterization in simulating tropical–extratropical dynamics in the SPCZ. For example, Song and Zhang (2018) showed that the prominent double-ITCZ bias in CESM1.2.1 could be eliminated by changing the convective scheme, producing a more realistic SPCZ. Changes in convective parameterization have also been reported to yield significant improvements in the simulated SPCZ in atmosphere-only simulations (L. Li et al., 2007; Wang et al., 2016). Niznik et al. (2015) suggested that parameterized physics in models, especially parameterized convection, is critical for understanding simulated precipitation in the SPCZ, and argued that the critical question is not whether waves interact with convection in models but how this interaction manifests and contributes to biases in the SPCZ.

In this paper, we compare two simulations using the National Center for Atmospheric Research (NCAR) Community Atmosphere Model version 5 (CAM5) with different convective parameterizations. The two simulations exhibit significant differences in the summertime SPCZ, allowing us to identify the physical mechanism by which parameterized convection alters the simulated SPCZ. We first investigate how the change in convection scheme affects the general circulation and distribution of precipitation over the SPCZ area. We then assess the vertical structure of diabatic heating in the SPCZ based on each simulation. Finally, in two steps, we provide a physical explanation for how the change in convective parameterization affects the intensity and variability of the simulated SPCZ. First, we perform an empirical orthogonal function (EOF) analysis of the SPCZ in both model runs, in which 'convective events' associated with tropical-extratropical interactions are defined. Second, we use a potential vorticity-based framework to diagnose the feedback between convection and transient waves that triggers the convective events.

In section 2, we describe the model, the two convective parameterizations, the data used for validation, and the analysis method. In section 3, we evaluate the simulated precipitation, circulation, and vertical structure of diabatic heating in the SPCZ region based on each convective scheme relative to observational and reanalysis-based benchmarks. In section 4, we explain the reasons why these two convective parameterizations produce such different simulations of the SPCZ. In section 5, we summarize the results and their implications.

2 Data and Methods

2.1 Model Simulations

All model simulations are conducted using the NCAR CAM5 (Neale et al., 2010; Hurrell et al., 2013), a global atmospheric GCM with 30 vertical levels. The physics step in CAM5 includes sequential application of the moist turbulence scheme developed by (Bechtold et al., 2008) and parameterized moist convection, followed by cloud macrophysics (Park, 2014) and microphysics (Morrison & Gettelman, 2008), and finally radiative transfer and chemistry. We use the default CAM5 physics package and the finite volume (FV) dynamical core at $1.9^{\circ}\times 2.58^{\circ}$ resolution (latitude×longitude).

Recently, Chu and Lin (2023) developed a new moist convection scheme that considers in-cloud inhomogeneity, in which the plume is divided into a series of interacting sub-plumes that mimic the transition from the convective core to the plume edge. Implementing this new scheme into CAM5 yielded distinct improvements in the simulated SPCZ relative to the default CAM5 run, especially during the austral summer (Chu & Lin, 2023). The standard deep convective parameterization in CAM5 is the Zhang–McFarlane scheme (hereafter referred to as ZM; G. Zhang & McFarlane, 1995) with a modified CAPE calculation that accounts for the effects of dilution by entrainment (Neale et al., 2008).

For this study, we conduct and compare simulations based on CAM5 with these two different representations of parameterized deep convection to better understand the dynamical mechanisms behind this change in the SPCZ. Two atmosphere-only simulations are carried out using the same prescribed sea surface temperature distributions: a default run with the original ZM (ORIG) and an experiment with the new convection scheme (NEW). Both simulations are run for 18 years. Results from the last 17 years are selected for further analysis, with the first year of each simulation discarded as spin-up.

2.2 Benchmark Data

Benchmark diagnostics for this study are based mainly on the ECMWF (European Centre for Medium-Range Weather Forecasts) fifth-generation reanalysis of the global atmosphere (ERA5; Hersbach et al., 2020). Daily-mean ERA5 products for 2000–2020 are used on a $1^{\circ}\times1^{\circ}$ latitude–longitude grid. Core variables for the analysis include precipitation, vertical pressure velocity at 500 hPa, and vertically-resolved atmospheric winds. Mean temperature tendencies due to physical parameterizations (mttpm) is also used to represent diabatic heating. Daily mean precipitation data for 2000–2022 from the Integrated Multi-satellitE Retrievals for GPM (IMERG) analysis are also used to set benchmarks for the spatio-temporal distributions of rainfall in the global tropics and in the SPCZ region.

2.3 Diabatic Potential Vorticity Production Rate

To quantitatively investigate the impact of diabatic heating on the atmospheric circulation, we use the potential vorticity (PV) production rate as described by Hoskins et al. (1985, their eq. 70a), which essentially represents the Lagrangian rate of change in local PV. After reformulating for pressure coordinates, the PV production rate is calculated as:

$$\frac{d\mathrm{PV}}{dt} = -g\left(\zeta_a \cdot \nabla_p H + K\nabla_p\theta\right) \tag{1}$$

The two terms on the right-hand side of equation 1 represent contributions from diabatic heating H and the curl of the frictional momentum tendency K, respectively. ζ_a represents the absolute vorticity, with ∇_p the gradient on isobaric coordinates. Focusing primarily on the influence of diabatic heating, we neglect the contribution of friction and keep only the vertical component of equation 1:

$$\mathrm{DPVR} = \left.\frac{d\mathrm{PV}}{dt}\right|_{\mathrm{diab}} = -g\left(\zeta_a \cdot \nabla_p H\right) = -g\left(\frac{\partial v}{\partial x} - \frac{\partial u}{\partial y} + f\right)\frac{\partial H}{\partial p} \tag{2}$$

where u and v are the zonal and meridional components of the local isobaric wind and f is the Coriolis parameter. Equation 2 indicates that the diabatic PV production rate (hereafter DPVR) is proportional to the absolute vorticity and the vertical gradient of diabatic heating. Previous studies have shown that DPVR provides a reliable measure of circulation anomalies that result from anomalous diabatic heating (Grams et al., 2011).

3 Impacts on the SPCZ

3.1 Precipitation

Both the ORIG and NEW simulations produce a diagonally-oriented SPCZ but with substantial differences in precipitation intensity. Mean precipitation rates during austral summer are underestimated along the climatological SPCZ axis in ORIG (solid black line in Figure 1a,e). This low bias in SPCZ intensity has previously been reported for simulations using the ZM convective parameterization and may be associated with the double-ITCZ bias (Wang et al., 2016; Song & Zhang, 2018; Chu & Lin, 2023). Replacing the ZM scheme with the new convective parameterization proposed by Chu and Lin (2023) eliminates much of the low bias in precipitation along the climatological axis of the SPCZ (Figure 1b,f). Differences in SPCZ intensity between the ORIG and NEW simulations strongly indicate that parameterized convection plays a critical role in simulating the SPCZ, as simply replacing the convection scheme increases rainfall in the SPCZ region by nearly 50% (Figure 1h). However, both model simulations and the ERA5 reanalysis overestimate precipitation in the ITCZ north of the equator, especially in its eastern branch (Figure 1e-g).

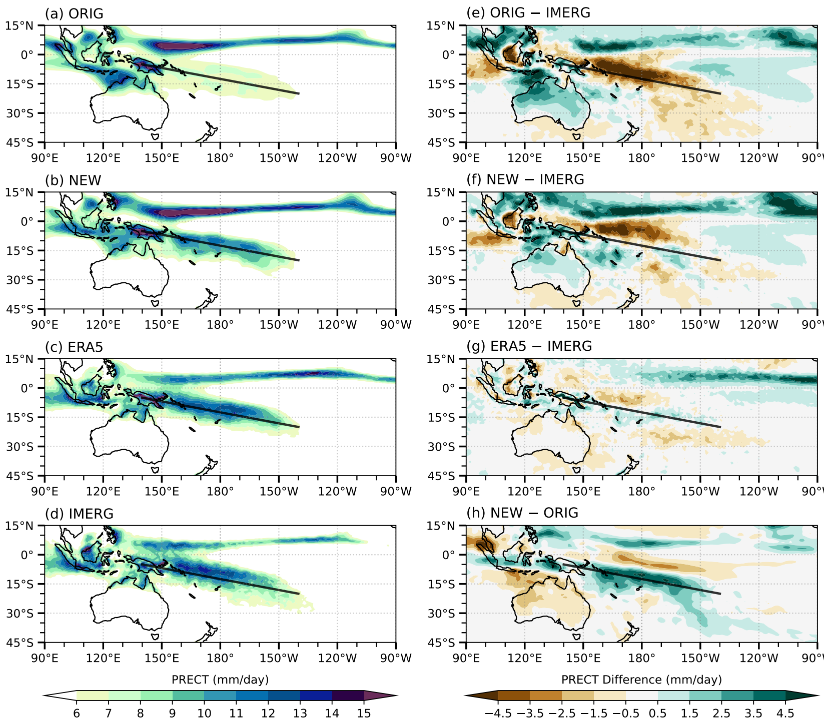

Figure 1. Seasonal-mean (December–February) distributions of precipitation based on (a) the ORIG simulation, (b) the NEW simulation, (c) the ERA5 reanalysis, and (d) the IMERG observational analysis; (e-f) biases in ORIG, NEW, and ERA5 precipitation relative to IMERG; and (g) the difference of NEW minus ORIG simulation results. The black solid line in each panel marks the climatological axis of the SPCZ during austral summer.

The increase in rainfall over the SPCZ region between the ORIG and NEW simulations results primarily from synoptic-scale convective rainfall rather than large-scale precipitation. Both convective and large-scale precipitation are essential contributors to tropical rainfall, but the former dominates SPCZ intensity (Figure S1a,b). Although changes in convective parameterizations can also lead to changes in large-scale rainfall (Y. Lin et al., 2013), increases in large-scale precipitation in NEW relative to ORIG are found mainly along the ITCZ and south of 30°S. By contrast, the distinct increase in convective precipitation along the SPCZ axis suggests that deep convection plays the dominant role in the improvement. Moreover, enhanced precipitation along the SPCZ occurs mainly at the synoptic time scale (≤ 14 day, Figure S2e-h), consistent with expectations for the contributions of transient eddies to rainfall in the SPCZ (Matthews, 2012; Niznik et al., 2015). As such, the reduced negative bias in precipitation intensity in NEW can be mainly attributed to changes in the representation of deep convection within the SPCZ.

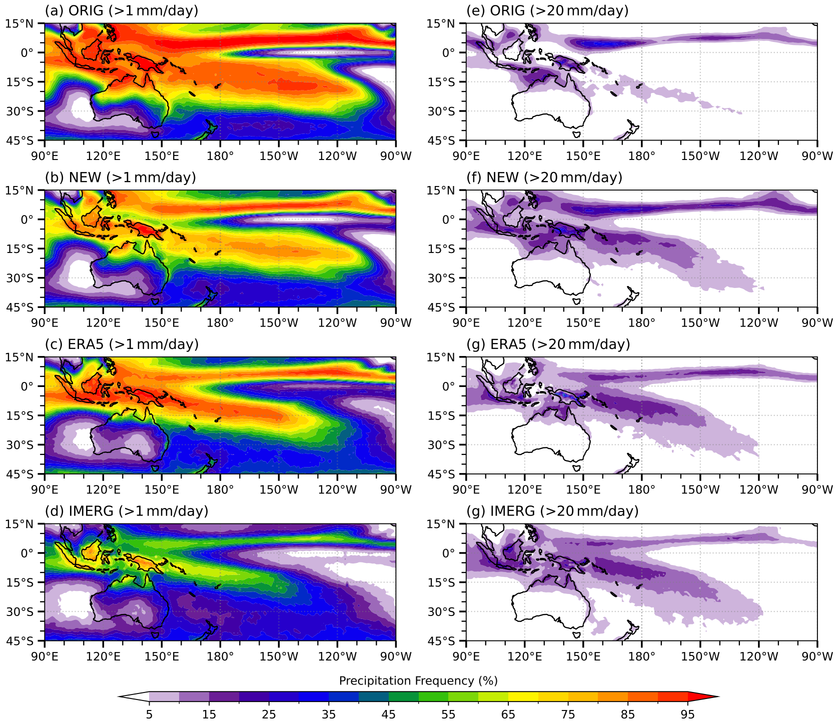

Figure 2. Spatial distributions of the frequency of daily-mean precipitation exceeding $1\,\mathrm{mm\,day^{-1}}$ (a-d) and $20\,\mathrm{mm\,day^{-1}}$ (e-g) during austral summer based on (a,e) the ORIG simulation, (b,f) the NEW simulation, (c,g) the ERA5 reanalysis, and (d,h) the IMERG observational analysis.

Figure 2 shows spatial distributions of rainy days (daily-mean rate $\geq 1\,\mathrm{mm\,day^{-1}}$) and heavy rain days (daily-mean rate $\geq 20\,\mathrm{mm\,day^{-1}}$) based on ORIG, NEW, ERA5, and IMERG. During austral summer, the ORIG simulation overestimates the frequency of precipitation (Figure 2a) by almost 50% relative to observations (Figure 2d). NEW and ERA5 also produce higher frequencies of rainy days relative to IMERG (Figure 2b,c), but the differences are reduced to around 20% in the SPCZ region, with NEW providing the closest match to observations. Meanwhile, the frequency of heavy rain days (≥ 20 mm/day) is greatly underestimated in ORIG (Figure 2e) relative to the observations (Figure 2g), especially along the SPCZ. This suggests that the weaker SPCZ in ORIG may result from an inability to accurately capture the occurrence frequency of heavy precipitation in the SPCZ region, particularly as heavy rain days account for roughly 70% of the total precipitation along the SPCZ. The new convection scheme (Figure 2f) mitigates the negative bias in heavy rain days, producing a much closer match to the reanalysis and observational products.

Figure 3a shows frequency distributions for precipitation during DJF over the SPCZ region (20°S-5°N, 150°W to 140°E) and the tropical Indo-Pacific (15°S-15°N, 90°W to 60°E) based on the ORIG and NEW simulations, the ERA5 reanalysis, and the IMERG observational analysis. Changes in precipitation between the ORIG and NEW simulations are not confined to the SPCZ region, as the ORIG simulation vastly underestimates heavy precipitation throughout the tropics . The frequency of daily mean precipitation greater than 20 mm day^{-1} decreases much faster in ORIG than in the observed distribution, and ORIG produces almost no days with precipitation greater than 50 mm/day (frequency $\leq$ 0.01%). As a result, light rain ($\leq$ 20 mm/day) constitutes nearly 90% of the total SPCZ rainfall in ORIG, more than twice the observed ratio (Figure 3b). Changing the convection scheme significantly reduces this negative bias in the frequency of precipitation rate. By contrast, the frequency distribution based on the NEW simulation exhibits a striking similarity to that based on ERA5 (solid red and black lines in Figure 3). Although both NEW and ERA5 still overestimate the contribution of light rain and underestimate the contribution of heavy rain relative to observations (Figure 3b), these gaps are greatly reduced relative to ORIG.

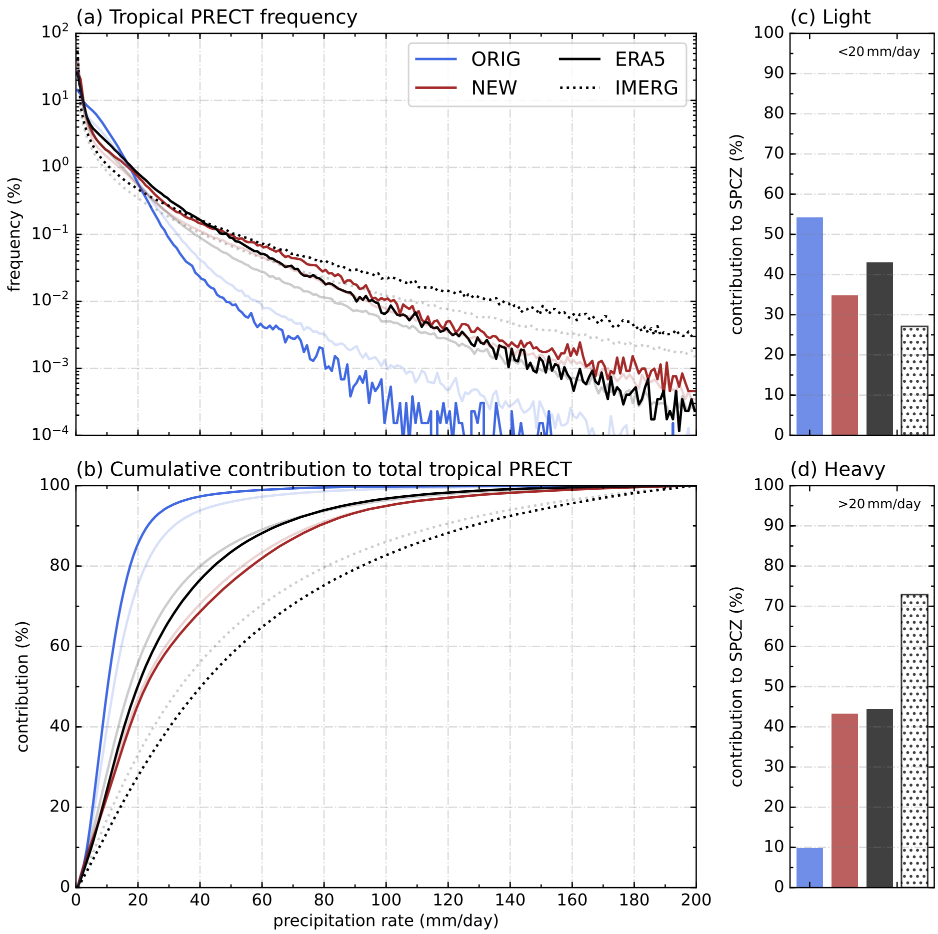

Figure 3. The left column shows (a) frequency distributions and (b) cumulative contributions to total precipitation as a function of daily-mean precipitation rate for the ORIG (blue) and NEW (red) simulations, the ERA5 reanalysis (black solid lines), and the IMERG observational analysis (black dotted lines). Heavy lines indicate distributions over the SPCZ region (20°S-5°N, 150°W to 140°E); lighter lines indicate distributions over the tropical Indo-Pacific (15°S-15°N, 90°W to 60°E). The right column shows contributions of (c) light ($\leq$20 mm/day) and (d) heavy ($\geq$20 mm/day) rain relative to precipitation in the SPCZ region. Contributions are normalized relative to IMERG, so that only the values based on IMERG are guaranteed to sum to 100%.

The underestimation of heavy rain in ORIG results from the well-known "too much drizzle" problem in the ZM convective parameterization (G. J. Zhang & Mu, 2005; J.-

L. Lin et al., 2006; Dai, 2006). During austral summer, more than 70% of the precipitation in the SPCZ region occurs on days with rainfall exceeding 20 mm day^{-1} (dotted bar in Figure 3c,d). Both simulations and ERA5 fail to fully capture this preference for heavy rain. Compared to IMERG, NEW and ERA5 both produce larger amounts of light precipitation and smaller amounts of heavy precipitation in the SPCZ domain. However, these differences are much smaller than those in ORIG, where precipitation occurring on heavy rain days accounts for less than 10% of total rainfall, a negative bias of more than 80% relative to observations. The relative weakness of the SPCZ in the ORIG simulation can therefore be attributed to a lack of heavy rainfall. Figure 3 indicates that this issue is even stronger along the SPCZ than in the tropical Indo-Pacific as a whole. Notably, all three of IMERG, ERA5, and NEW indicate that the frequency of rainy days in the SPCZ exceeds that in the tropical Indo-Pacific (Fig. 3a), with greater fractions of total precipitation contributed by light rain (Fig. 3b). ORIG produces the opposite relationship, with heavy rain contributing more to total precipitation in the tropical Indo-Pacific than in the SPCZ region. A realistic simulation of the SPCZ requires an accurate representation of the precipitation distribution, especially the contribution of heavy rainfall.

To summarize, the intensity of SPCZ precipitation is greatly underestimated by the ORIG simulation, primarily due to a lack of heavy rainfall associated with deep convection. This can be partly explained by the well-known lack of intense precipitation in models using the ZM convective scheme (G. J. Zhang & Mu, 2005; J.-L. Lin et al., 2006). However, as this deficiency is intrinsic to ORIG, it is unclear why the bias is amplified specifically over the SPCZ region. The NEW simulation produces a much better match to reanalysis products and observations in both the intensity of the SPCZ and the contribution of heavy precipitation to total precipitation in the SPCZ region. The main question now is to identify the mechanism behind the large discrepancy between the two model simulations of convective rainfall along the SPCZ. We revisit this question in detail in section 4.

3.2 Vertical Diabatic Heating Structure

Diabatic heating is a crucial component of the dynamics of tropical–extratropical interactions in the SPCZ due to the vortex-stretching effects of strong latent heat release (Matthews, 2012; van der Wiel et al., 2016a). By artificially suppressing this mechanism, van der Wiel et al. (2016a) showed that it contributes significantly to wave-induced precipitation in the SPCZ. Diabatic heating in CAM5 is represented by the sum of solar heating (QRS), longwave heating (QRL), the temperature tendency due to moist processes (DTCOND), and the temperature tendency due to vertical diffusion (DTV). A comparable estimate from ERA5 is provided by the mean temperature tendency due to parametrizations (mttpm; Hersbach, Bell, Berrisford, Hirahara, et al., 2017). Apparent heat sources following Yanai et al. (1973) have also been calculated from analyzed dynamical fields based on ERA5. Results based on this approach are similar to those based on diabatic heating from the forecast model (Figure S3a).

Figure 4a shows vertical profiles of diabatic heating associated with deep convective rainfall exceeding 8 mm day^{-1} in ORIG, NEW, and ERA5. Heating based on the ORIG simulation is smaller in magnitude and shifted toward lower altitudes relative to ERA5 (Figure 4a). Although both ORIG and NEW show top-heavy structures, larger heating at mid-levels (400–600 hPa) in NEW results in a vertical distribution that better matches that in ERA5. The temperature tendency due to moist physics is dominant among the four components of diabatic heating (Figure S3b), confirming the central role of moist convection. Normalizing the heating profile relative to precipitation (Figure 4b) further shows that ORIG underestimates upper-level heating relative to ERA5 (Figure 4b), even for precipitation events of the same magnitude. This bias is reduced near 400 hPa in the NEW simulation, although NEW still underestimates heating relative to ERA5 in the deep convective detrainment layer (200–300 hPa).

Underestimating the magnitude and altitude of heating reduces the vertical gradient of diabatic heating ($\partial H/\partial z$) in the upper troposphere. This bias essentially throttles the extent to which parameterized convection can influence its dynamical environment in ORIG, as a smaller vertical gradient of diabatic heating inevitably reduces the diabatic potential vorticity production rate (DPVR; eq. 2). The impact of this reduction in DPVR on Rossby waves propagating through the SPCZ region is discussed further in section 4. The vertical profile of diabatic heating based on ERA5 (Figure 5) shows two distinct peaks, with a local minimum near 600 hPa. This pattern has also been noted by Hagos et al. (2010), who reported that the exact vertical location and amplitude of this secondary peak varied among different products, in contrast to the primary peak in the upper troposphere (Hagos et al., 2010, their Fig. 3).

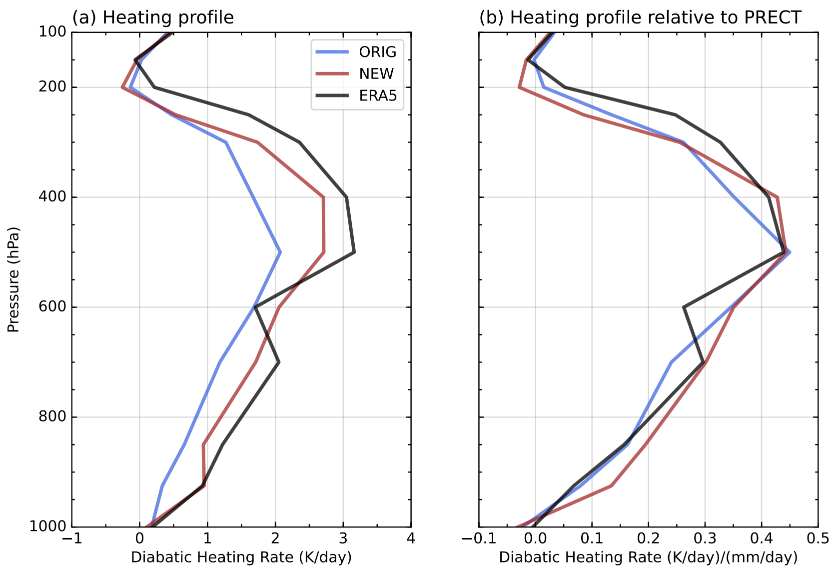

Figure 4. Mean profiles of (a) diabatic heating and (b) diabatic heating normalized by precipitation rate averaged over the SPCZ region (20°S-5°N, 150°W to 140°E) for days with precipitation exceeding 8 mm day^{-1}.

To better distinguish between light rain and heavy rain days, the upper panels of Figure 5 show variations in the vertical profile of diabatic heating as a function of precipitation rate for ORIG, NEW, and ERA5. Daily-mean precipitation rates are separated into 50 bins from 0.01 mm day^{-1} to 1000 mm day^{-1}, with frequency density functions as shown in the lower panels of Figure 5. The regional-mean heating profile in each bin is normalized (divided by the square root of the sum of the squared heating at all levels). Normalized diabatic heating profiles corresponding to different precipitation rates show how the vertical distribution of positive and negative heating changes with increasing rainfall.

The heating structure displays three patterns that we label as suppressed, disturbed, and mature convective conditions. When convection is suppressed (precipitation ≤ 1 mm day^{-1}), positive heating is restricted to the surface with two layers of strong radiative cooling in the lower and upper troposphere, respectively. The region of positive heating ascends with increasing precipitation rates between 1 mm day^{-1} and 10 mm day^{-1}. The shift of the heating profile from bottom-heavy to top-heavy indicates a transition from shallow convection to deep convection over this range of precipitation rates (Hagos et al., 2010). The distinct peak of negative diabatic heating in the upper troposphere (around 400–500 hPa) persists up to precipitation rates of $\sim$4 mm day^{-1}, possibly due to radiative cooling at the tops of shallow convective cumulus clouds. Mature convection conditions are characterized by top-heavy heating that peaks around 400 hPa. Indications that this level of peak heating descends toward lower altitudes during extreme precipitation events ($\geq$ 100 mm/day) may result from increasing contributions of large-scale relative to convective precipitation.

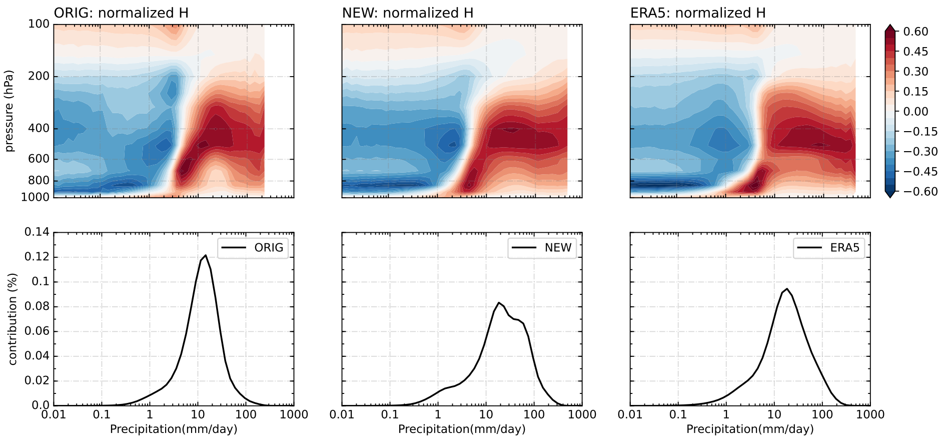

Figure 5. Variations of (upper) normalized vertical profiles of diabatic heating (H_{norm}) and (lower) contributions to total precipitation as a function of area-mean daily precipitation in the SPCZ region (20°S-5°N, 150°W to 140°E). Daily-mean precipitation rates are divided into 50 bins, and the diabatic heating rates are normalized by dividing the mean profile in each bin by the square root of the sum of squared heating at all levels.

Although both simulations capture the increasing elevation of positive heating with increasing precipitation rate, their structures differ in some critical details. The most obvious difference occurs during the transition from shallow convection to deep convection (1–10 mm day^{-1}; upper panels of Figure 5). For precipitation rates less than 8 mm day^{-1}, ORIG produces weaker heating in the lower troposphere ($\sim$850 hPa) relative to ERA5. This difference is largely eliminated by replacing the original ZM scheme with the new convection scheme. For precipitation rates greater than 8 mm day^{-1}, ORIG exhibits an intense mid-level center of positive heating that shifts upward as convection matures. However, the sharp peak in precipitation rates slightly larger than 10 mm day^{-1} and the lack of a distinct peak in lower tropospheric heating below this threshold suggest that deep convective activity suppresses shallow convection in ORIG, ultimately resulting in deep convection that is both too frequent and too weak. This tendency for deep convection to occur too frequently may suppress shallow convective moistening of the lower troposphere (Del Genio et al., 2012; Q. Cai et al., 2013; Wright et al., 2017), further limiting the intensity of deep convection. In addition, the height of the maximum heating begins to descend with increasing precipitation at a smaller precipitation rate ($\sim$20 mm day^{-1}) than in the reanalysis, indicating a narrow distribution of deep convective precipitation rates in this simulation. By contrast, results for the NEW simulation show a strong similarity with the reanalysis in almost all aspects, with the exception of slightly weaker heating above 300 hPa at precipitation rates near 10 mm day^{-1}.

Heating profiles based on the ORIG simulation are unsurprisingly weak and low in the SPCZ region (Fig. 4; upper panels of Fig. 5) given the lack of intense precipitation in this model (lower panels of Fig. 5). The center of positive heating corresponding to the peak precipitation rate in ORIG ($\sim$10.5 mm day^{-1}) is shifted toward lower altitudes relative to those in NEW and ERA5. This difference indicates that the lack of heavy rain days reduces not only the magnitude of heating but also the altitude at which this heating takes place, thereby inhibiting convective influences on the upper-level circulation.

3.3 General Circulation

Figure 6 shows spatial distributions of low-level (925 hPa) divergence in ORIG, NEW, and ERA5, along with differences between these products. Low-level convergence is a crucial moisture source for local convection in the SPCZ (Takahashi & Battisti, 2007; Lintner & Neelin, 2008). Convergence in this region based on the ORIG simulation is weak and characterized by two distinct bands, one located along the main axis of the SPCZ and the other closer to the equator (Figure 6a). The convergence band closer to the equator is likely related to the double-ITCZ bias. The negative bias in convergence relative to ERA5 results from a southeasterly bias in low-level winds along the northern edge of the SPCZ axis (Figure 6d). This bias in the low-level winds indicates reduced low-level inflow and is directly linked to the existence of the second (equatorward-shifted) band of convergence in the lower troposphere. The NEW simulation shows distinct increases in northwesterly winds along virtually the entire SPCZ axis relative to ORIG, resulting in a dipole pattern in the difference between the two model simulations (Figure 6f). These differences show that replacing the convective parameterization also changes the large-scale distribution of convergence in the lower troposphere. However, the NEW simulation also shows biases in low-level winds relative to ERA5, especially along the equator. The bias in NEW manifests as stronger trade winds over the western tropical Pacific and slightly weaker convergence along the northeastern flank of the SPCZ, and is consistent with a negative precipitation bias in this region (Fig. 1f).

The low-level wind field is largely determined by the horizontal temperature gradient in the lower troposphere. Weaker northwesterly winds in ORIG may therefore be attributed to a negative temperature anomaly in the SPCZ region (Figure S4 and Kun et al., 2010), consistent with differences in diabatic heating (Figure 4). Diabatic heating in the lower troposphere (800–900 hPa) is weak in ORIG due to the lack of shallow convective heating. Stronger low-level heating in NEW and ERA5 helps to draw moist inflow from the tropics, increasing local convergence and priming the atmosphere for deep convection. This heating intensifies and rises toward higher altitudes as convection strengthens, in a positive feedback loop that reinforces low-level convergence. The low-level warming then transitions to cooling as convection strengthens, dampening the feedback loop (Figure 5) and allowing instability to begin to build again. The unrealistically narrow distribution of precipitation in the ORIG simulation results in both weaker low-level heating (due to the lack of shallow convection) and weaker upper-level heating (due to the lack of heavy precipitation), which both conspire to reduce inflow from the equator. This reduced inflow weakens convergence in the SPCZ region, limiting the intensity of SPCZ precipitation. Moreover, because the bias in heavy precipitation is smaller in the equatorial region, the convergence zone is not only suppressed in the SPCZ region but also drawn toward the more favorable conditions along the equator, ultimately resulting in a double ITCZ.

The upper tropospheric circulation also plays a critical role in determining the characteristics of tropical–extratropical interactions in the SPCZ (Matthews, 2012; van der Wiel et al., 2015). Figure 7 shows distributions of zonal wind on the 200 hPa isobaric surface. The two simulations show distinct differences in the tropics, particularly in the 'westerly duct' region over the eastern equatorial Pacific (Hoskins & Ambrizzi, 1993). Easterly winds over the maritime continent are also weaker and shifted westward in ORIG relative to NEW (red contours in Figure 7). A smaller shift is also evident in the west-

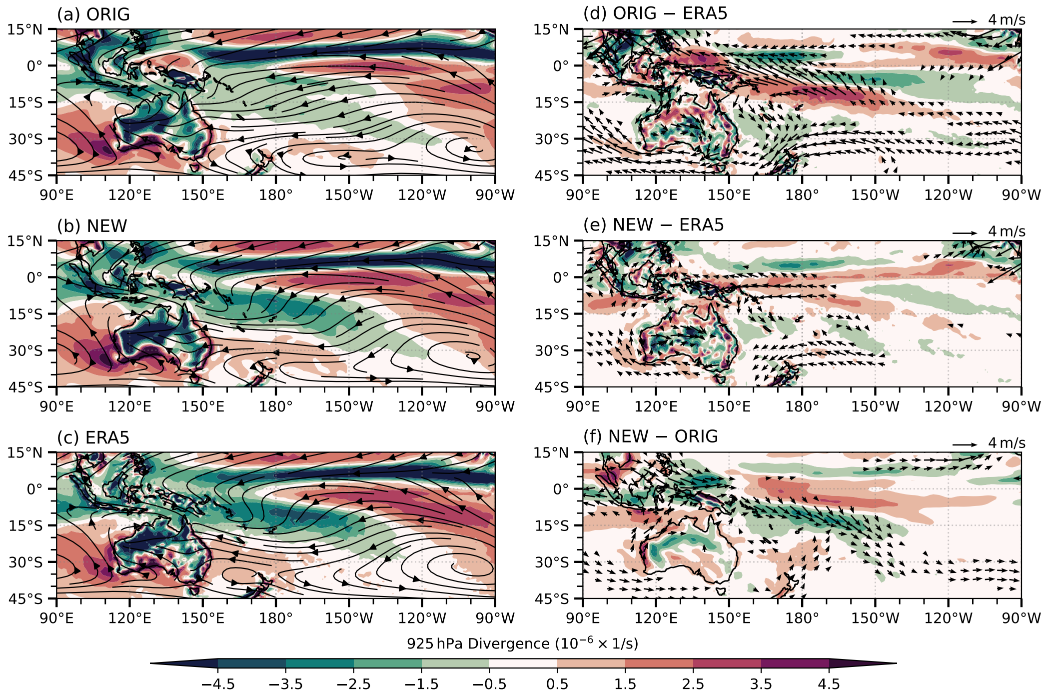

Figure 6. Seasonal-mean (DJF) spatial distributions of divergence and wind streamlines on the 925 hPa isobaric surface based on (a) ORIG, (b) NEW, and (c) ERA5, along with differences between (d) ORIG minus ERA5, (e) NEW minus ERA5, and (f) NEW minus ORIG.

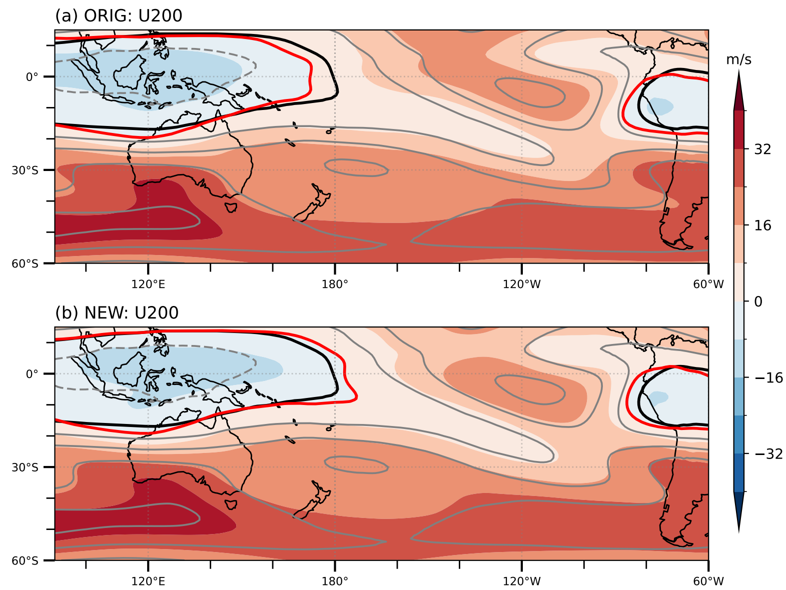

Figure 7. Climatological-mean 200 hPa zonal winds (U200; shading) based on (a) ORIG and (b) NEW during austral summer (DJF). Contours show the U200 climatology from ERA5 with the same intervals as the shading. Solid lines mark the zero contours in ERA5 (black) and model outputs (red), respectively, delineating the westerly duct (see text for details).

ern boundary of the easterlies over tropical South America. These changes widen the westerly duct and shift it westward in ORIG relative to NEW. The westerly duct in NEW is weak and narrow by comparison (Figure 7b). Differences in the strength and location of the westerly duct between ORIG and NEW can be attributed to stronger westerly winds in ORIG, which can be at least partially explained by reduced diabatic heating in the SPCZ (van der Wiel et al., 2016a). Variations in the structure of the westerly duct modulate the frequency of equatorward-refracted transient waves and tropical–extratropical interactions in the SPCZ (Matthews, 2012), as discussed in the following section.

4 Wave-convection feedback

4.1 Convective Events over SPCZ

The SPCZ has been referred to as a 'graveyard' for extratropical weather systems due to its tendency to dissipate fronts entering the region from the southwest (D. G. Vincent, 1994). This tendency also reflects the close connection between the SPCZ and transient Rossby waves. During the austral summer, vorticity gradients in the background flow cause Rossby waves propagating along the Southern Hemisphere westerly wave guide to be refracted from the jet exit region near New Zealand towards the westerly duct over the equator (van der Wiel et al., 2015). When passing through the SPCZ, these synoptic eddies often dissipate and trigger bursts of diagonally oriented convection, or 'convective events' (Matthews, 2012; van der Wiel et al., 2016a; Brown et al., 2020). To reproduce this variability, models must reliably simulate the relevant dynamic and thermodynamic processes.

Table 1. Number of convective events, days, and average duration[a]

	Events (per year)	Days (per year)	duration (per event)
ORIG	11.3	15.1	1.3
NEW	10.0	12.7	1.3
ERA5	9.3	13.4	1.4

[a]See section 4.1 for definitions.

To identify convective events, empirical orthogonal function (EOF) analysis is applied to vertical velocity anomalies on the 500 hPa isobaric surface within 5°S–25°S and 160°E–150°W (grey dash-dot box in Figure 8). The vertical velocity at 500 hPa (W500) is an alternative indicator of outgoing longwave (OLR) and is often used to study the dynamics of convergence zones (e.g., De Almeida et al., 2007). The first EOF mode (EOF-1) is characterized by strong updrafts and downdrafts on the northeastern and southwestern flanks of the subtropical SPCZ axis (Figure 8), indicating that EOF-1 is associated with north–south shifts of the subtropical SPCZ. This shifted SPCZ mode, which is caused by the passage of upper-level transient waves (Matthews, 2012), defines the statistics of 'convective events' listed in Table 1. A wider westerly duct, as in ORIG (Fig. 7), causes more transient eddies to be refracted toward the eastern equatorial Pacific, resulting in more convective events in the SPCZ region. Conversely, convective events decrease when the westerly duct is compressed. Accordingly, about 1.3 fewer events occur per austral summer in NEW than in ORIG (Table 1). The smaller numbers of convective events and convective event days in NEW are more consistent with those based on the ERA5 reanalysis (Table 1), despite NEW producing a narrower westerly duct than ERA5.

The center of convection in EOF-1 based on ORIG (Figure 8a) is smaller and located further toward the southwest compared to the reanalysis (Figure 8c). Although

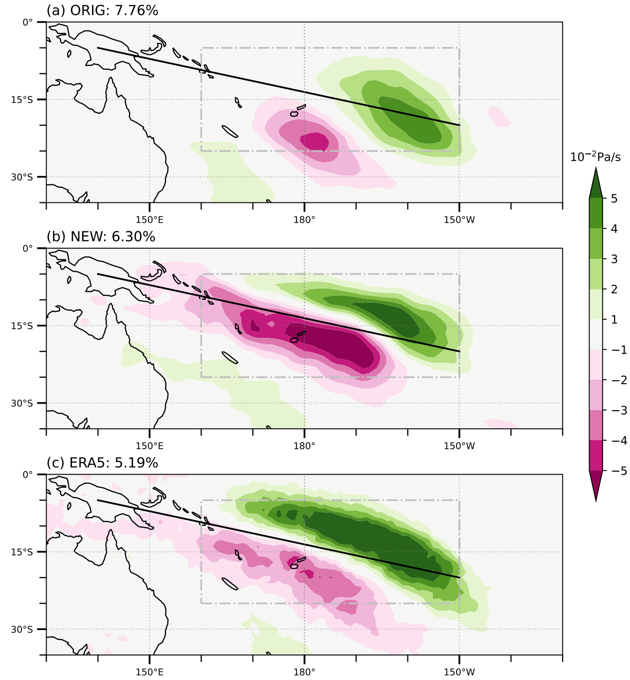

Figure 8. The first mode of EOF analysis applied to pressure vertical velocity anomalies on the 500 hPa isobaric surface (W500) within 5°S–25°S and 160°E–150°W (grey dash-dot box) in (a) ORIG, (b) NEW, and (c) ERA5. The black solid line marks the axis of the SPCZ.

ORIG produces more convective events (Table 1), these events are associated with relatively weak vertical velocity anomalies, indicating a more limited response to upper-level waves (Figure 8a). Vertical velocity anomalies associated with convective events in NEW are more similar to ERA5 in both intensity and spatial distribution (Figure 8b). Moreover, the northwestward expansion of anomalous updrafts along the main axis of SPCZ reported by some previous studies (e.g., Niznik et al., 2015) is only seen in NEW and ERA5, with little evidence of expanded convection in ORIG. In the following analysis, 'convective days' indicate days for which the first principal component exceeds one standard deviation ($PC1 \geq 1$). Following van der Wiel et al. (2016a), composite distributions are constructed around the day when PC1 reached its maximum during the event.

Atmospheric wave patterns are often diagnosed as anomalies in meridional winds on the 200 hPa isobaric surface (V200) in the upper troposphere (Z. Lin, 2019; Senapati et al., 2022). Figure 9 shows how these patterns relate to precipitation anomalies on convective event days (day 0) and the days immediately preceding (day –1) and following (day +1) these days. On day –1, transient waves in the westerly wave guide (around 50°S) are refracted toward the tropics (purple line in Figure 9) by the local meridional vorticity gradient, triggering bursts of convection within the SPCZ (van der Wiel et al., 2015). On the day of the convective event (day 0 in Figure 9), there is an upper-level anticyclonic anomaly straddling the axis of the SPCZ, near where the purple and black lines intersect. This upper-level anticyclonic anomaly is associated with quasi-isentropic ascent in the southern part of the SPCZ and descent in the northern part of the SPCZ, intensifying convection in the south and suppressing convection in the north (Matthews, 2012).

Although both ORIG and NEW capture the equatorward refraction of waves, the strength of the corresponding convective events is quite different. Wave-induced rain-

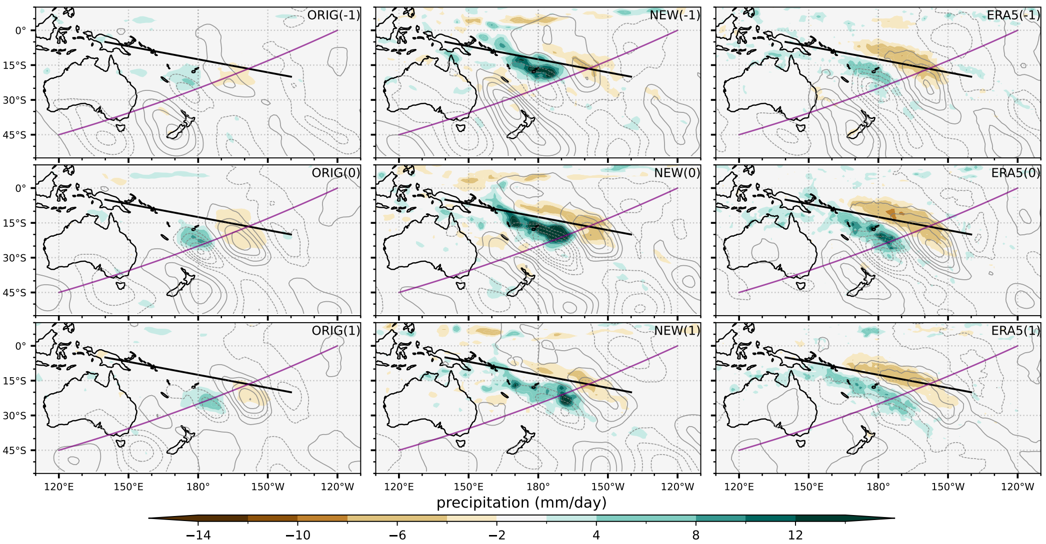

Figure 9. Composite-mean anomalies of precipitation (shading) and 200 hPa meridional winds (contours) from (left) ORIG, (center) NEW, and (right) ERA5 on (upper row) day –1, (middle row) day 0, and (lower row) day +1 of convective events. The solid black line marks the SPCZ axis, while the solid purple line denotes an approximate wave propagation path. The contour interval for meridional wind anomalies is $1.6\,\mathrm{m\,s^{-1}}$, with negative contours dashed and the zero contour omitted.

fall anomalies (shading in Figure 9) are much weaker in ORIG than in NEW throughout the event. Despite similar circulation anomalies in the refracted wave, ORIG produces rainfall anomalies much weaker than those in ERA5, while NEW produces anomalies that are slightly stronger than those in ERA5. These discrepancies between ORIG and NEW result from differences in the vertical structure of convection as represented by the convective parameterization. Specifically, the wave becomes distorted as it passes through the SPCZ in NEW, losing its regular shape and extending toward the tropics. A similar distortion is seen in the reanalysis, but is largely absent in ORIG. The wave deformation seen in NEW and ERA5 is consistent with the expansion of updrafts in Figure 8 and leads to more persistent local updrafts and enhanced convection along a larger segment of the SPCZ axis.

During convective events, the precipitation distribution shifts towards heavy rainfall (Figure 10a-c). This shift indicates that transient waves amplify the intensity of convection during convective events, increasing the likelihood of heavy rain. However, the shift in the precipitation peak in ORIG is small relative to that in the reanalysis, while NEW produces a slightly larger shift than that indicated by ERA5. During convective events, contributions to SPCZ precipitation in ORIG remain concentrated around $10\,\mathrm{mm\,day^{-1}}$. Larger precipitation rates ($\geq 20\,\mathrm{mm}$) are rarely produced in ORIG even during convective events, with contributions at these rates less than half of those in ERA5 (Figure 10d). This bias is clearly reduced in the NEW simulation, which shows significant increases in heavy rainfall as the peak of the distribution shifts from near $20\,\mathrm{mm\,day^{-1}}$ to $80\,\mathrm{mm\,day^{-1}}$ (Figure 10d). Although NEW overestimates the occurrence of extremely heavy rain ($\geq$50 mm/day) relative to ERA5 (Figure 10e), the general distribution based on NEW is similar to that based on the reanalysis ((Figure 10d). As the vertical distribution of diabatic heating depends in large part on precipitation rate (i.e., Figure 5), interactions between convection and transient waves are likely to feature more prominently in NEW.

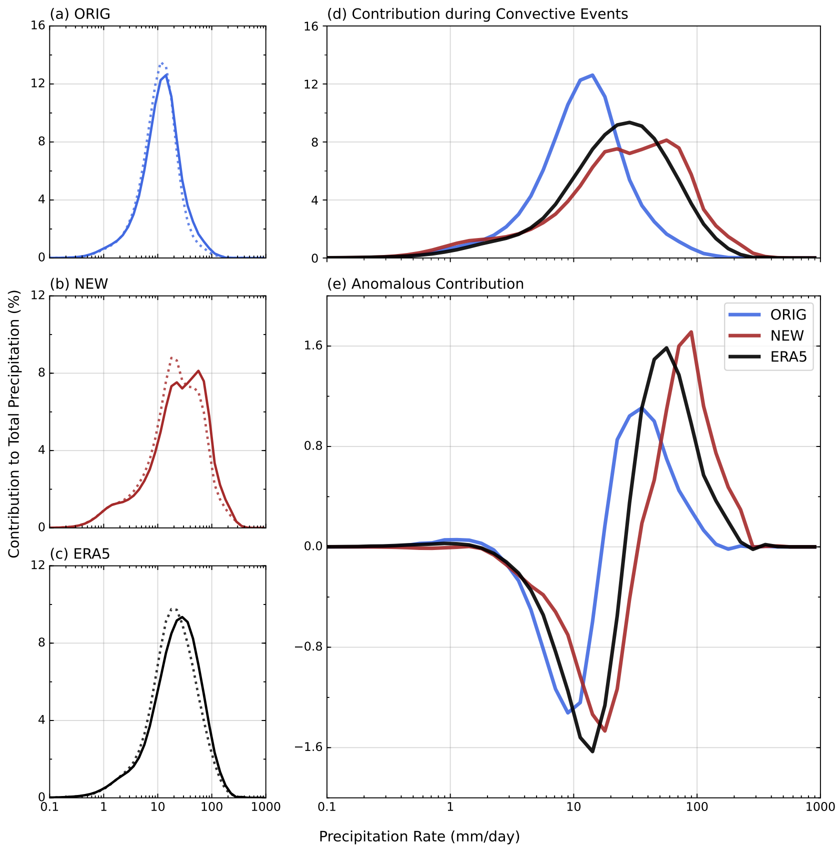

Figure 10. Contributions of different precipitation rates to total precipitation in the SPCZ region in (a) ORIG, (b) NEW, and (c) ERA5 on all days (dotted lines) and convective event days (solid lines). (d) Distributions of precipitation rate during convective events and (e) anomalous contributions relative to the distribution on all austral summer days for ORIG (blue), NEW (red), and ERA5 (black).

4.2 Role of Diabatic Heating

Figure 11 shows composite-mean vertical cross-sections for the transient waves that initiate convective events, averaged within ±3° latitude of the wave track (purple lines in Figure 9). Waves in both simulations exhibit a clear baroclinic structure, with the largest anomalies in meridional winds centered around 200 hPa, near the tropopause, and an evident westward tilt. The 'graveyard' nature of the SPCZ is evident in the distortion of the wave signals along these tracks. Distinct patterns of anomalous diabatic heating (purple contours in Figure 11) emerge along the SPCZ axis, beneath the anticyclonic anomaly in the upper-level wind. These anomalies in diabatic heating correspond to anomalous latent heat release during the convective event.

Near the longitude of the central SPCZ axis (black line in Figure 11), the waves are distorted by mid-level diabatic heating (Matthews, 2012; van der Wiel et al., 2016a). Intensification of the vertical gradient of diabatic heating ($\partial H/\partial p$, Equation 2) near 300 hPa yields positive diabatic potential vorticity production rates (DPVRs) in the upper troposphere (shading in Figure 11). The associated increase in potential vorticity opposes the upstream cyclonic anomaly and elongates the transient eddies along the SPCZ axis. At lower levels, negative DPVRs induce cyclonic circulation anomalies and intensify convergence, resulting in changes in the tilt structure around 175 °E (Figure 11). Consequently, the vertical DPVR dipole generates a secondary circulation that amplifies the downstream anomaly while opposing the upstream anomaly, distorting the wave and preventing it from continuously propagating. Feedback between waves and convection also lifts and sharpens the wave-induced circulation anomalies toward the tropopause as they pass through the SPCZ region. The wave signal is thus more concentrated and confined to the upper troposphere downstream of the SPCZ.

Both the ORIG and NEW simulations capture elements of the transient wave–convection feedback (Figure 11)a,b), but the intensity of this feedback is substantially weaker in ORIG than in NEW. ORIG shows the weakest diabatic heating among the three products, with peak values only about half of those in NEW despite a similar wave forcing. Such a small heating signal implies a weaker local convective response to wave-induced uplift, consistent with lighter rain during convective events in ORIG (Figure 9). This weak upper-level heating leads to smaller values of both positive DPVR around 300 hPa and negative DPVR around 600 hPa compared to ERA5 and NEW. As a consequence, wave–convection feedback exerts a much weaker influence on transient eddies as they pass through the SPCZ. This results in waves propagating more continuously through the region and limits the amount of energy the SPCZ can extract from local dissipation of transient eddies, ultimately reducing the intensity of the SPCZ. Therefore, deficiencies in the ZM convective parameterization in the ORIG simulation not only limit precipitation in the SPCZ by directly reducing the frequency of heavy precipitation, but also prevent the model from accurately reproducing the amplifying effects of wave–convection feedbacks during the passage of transient waves. By contrast, wave–convection feedback in the NEW simulation is even stronger than that in the reanalysis. Large positive DPVRs are produced in the convective detrainment layer, while negative DPVRs stretch downward from 500 hPa to the surface. These anomalies lead to a stronger amplification of the wave-induced lower tropospheric convergence and upper tropospheric divergence than in the ORIG simulation. The clear upward shift of the wave center from 250 hPa to 150 hPa around 160°W further emphasizes the strength of the wave–convection feedback in NEW (Figure 11b). van der Wiel et al. (2016a) suggested that convective heating triggered by transient eddies in the SPCZ should weaken both the equatorial low-level flow and the upper-level westerly duct, leading to more vigorous convection over the SPCZ and less frequent wave refraction to the tropics. This is consistent with NEW producing fewer but stronger convective events than ORIG (Table 1).

Figure 12 shows Hovmöller diagrams of meridional wind and DPVR anomalies along the wave track, which provide an even clearer perspective on the effects of wave–convection

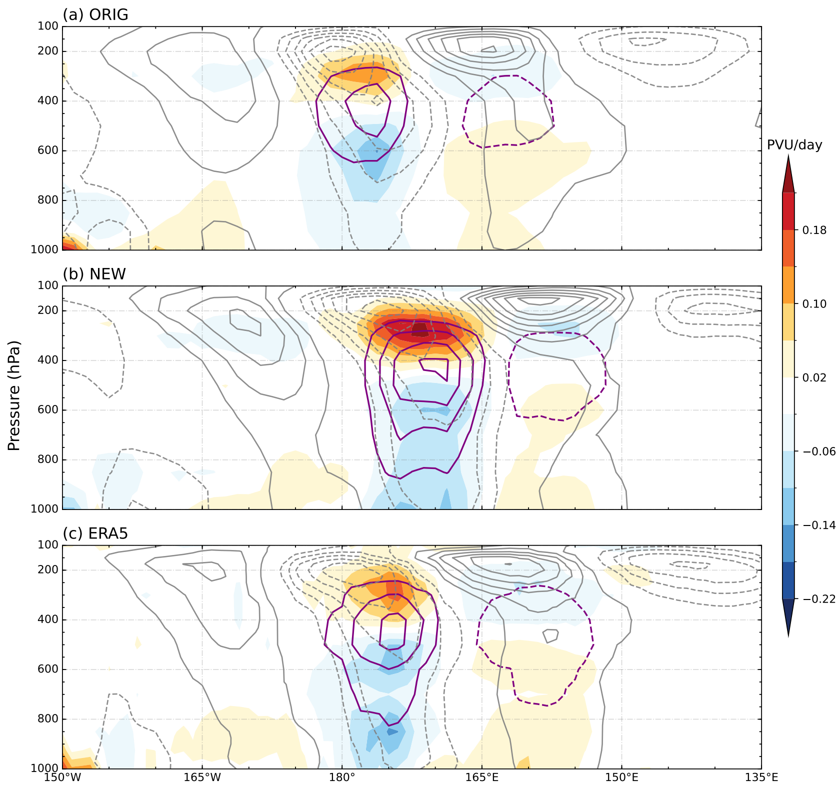

Figure 11. Cross-sections of anomalous diabatic potential vorticity production rate (shading), meridional winds (gray contours at 1-m/s intervals), and diabatic heating rate (purple contours at 2-K/day intervals) along the pathway of waves (purple curved lines in Figure 9) of (a) ORI, (b) NEW, and (c) ERA-5.

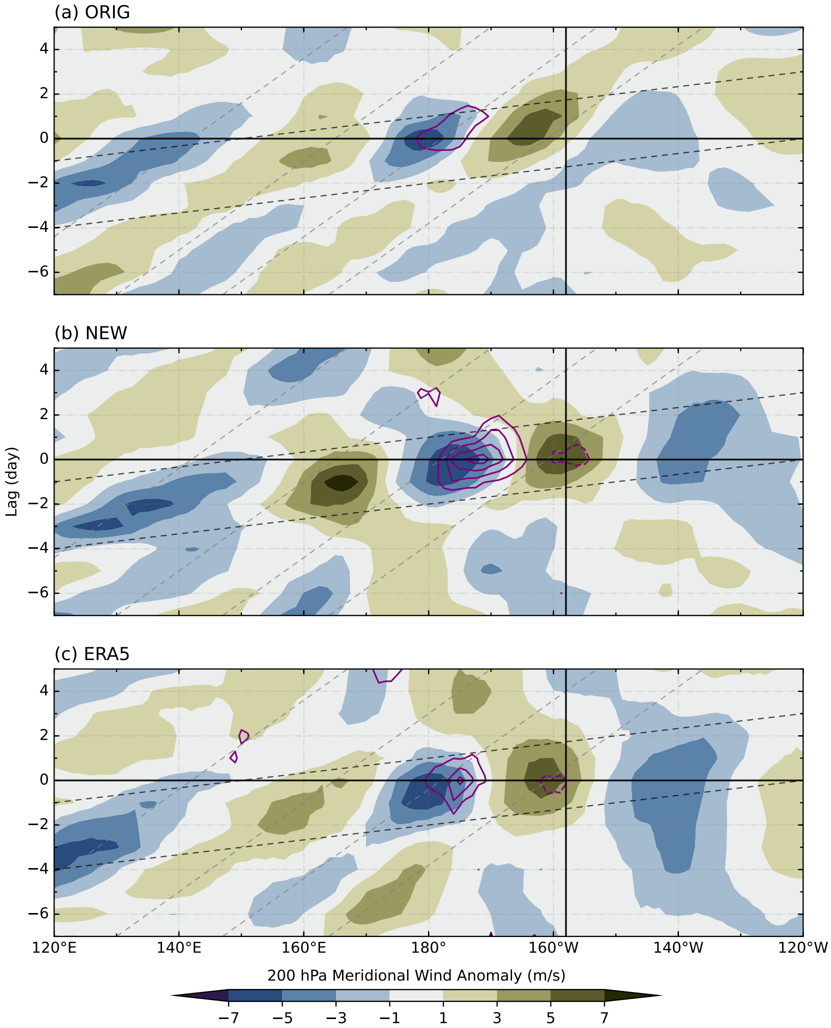

Figure 12. Hovmöller diagrams of composite-mean lagged anomalies of 200 hPa meridional winds (shading) and 250 hPa DPVR (contours) along the wave pathway (purple lines in Figure 9) based on (a) ORIG, (b) NEW, and (c) ERA-5. The DPVR contour interval is 0.6 PVU day^{-1}, with dashed contours for negative values and the zero contour omitted. The dotted lines show the approximate phase speed (grey) and group speed (black) in ERA5, the vertical solid line indicates the position of the mean SPCZ axis, and the thick horizontal line marks day 0.

feedbacks. ORIG, NEW, and ERA5 all show distinct eastward propagation of transient eddies, with a phase speed of about $6.5\,\mathrm{m\,s^{-1}}$ in ERA5 (grey dotted lines in Fig. 12). The wave energy moves at the substantially faster group speed of about $22.3\,\mathrm{m\,s^{-1}}$ (black dotted line in Figure 12), consistent with downstream development (Chang, 1993). The phase speed in NEW is slightly slower than that in ORIG or ERA5, probably owing stronger coupling with convection (Figure 11b). The phase speed and persistence of the signals decrease as the waves approach the SPCZ (black line in Figure 12), followed by dissipation around 140°W. Distinct positive DPVRs show up ahead of the propagating cyclone (purple contours in Figure 12), corresponding to the amplified upper-tropospheric divergence that tends to distort the original waves. The most pronounced difference between the simulations is found east of the mean SPCZ axis around 160°E. Quasi-stationary signals appear downstream of the strong positive DPVR anomalies in NEW and ERA5, corresponding to persistent local anomalies. However, the weaker DPVR anomaly in ORIG inhibits convective modulation of the upper-level circulation and allows transient waves around 160°W to maintain their eastward phase speed and continue propagating downstream. In addition to the difference in phase speed, the lifespan of eddies in ORIG is significantly longer than in NEW or ERA5, apparently inconsistent with the 'frontal graveyard' nature of the SPCZ. Indeed, the ORIG simulation bears striking similarities to the climatological diabatic heating experiments conducted by van der Wiel et al. (2016a). Weak westward motion in NEW and ERA5 at positive lags is caused by equatorward propagation of anomalous convection during convective events (Niznik et al., 2015) and is correspondingly absent from ORIG.

5 Conclusions and Discussion

In this study, the role of parameterized convection in simulating the South Pacific Convergence Zone (SPCZ) is investigated in the NCAR CAM5. Two simulations are conducted, one using the original ZM convective parameterization (ORIG) and the other using a new convection scheme (NEW; Chu & Lin, 2023) that produces a more realistic SPCZ (NEW) while keeping all other model settings the same. The ORIG simulation produces a very weak SPCZ during austral summer (DJF), which is significantly improved in NEW. The negative bias in SPCZ intensity in ORIG results both directly and indirectly from the ZM parameterization's well-known inability to produce enough intense precipitation (G. J. Zhang & Mu, 2005; J.-L. Lin et al., 2006). Specifically, the ORIG simulation produces too much light rain ($\leq$20 mm/day) but too little heavy rain ($\geq$20 mm/day), with heavy precipitation comprising 70% of total precipitation in the SPCZ region in observations but only about 15% in ORIG. This deficiency is even stronger in the SPCZ region than in the tropical Indo-Pacific as a whole. It is therefore not surprising that the ORIG simulation greatly underestimates the intensity of the SPCZ.

Upper-level diabatic heating in the SPCZ is weaker and shifted toward lower altitudes in ORIG, with a magnitude roughly half that in the ERA5 reanalysis. Consequently, the ORIG simulation produces smaller vertical gradients in diabatic heating, limiting the extent to which convection can modulate the upper-level circulation, including the circulation anomalies associated with transient Rossby waves that pass through the SPCZ (Equation 2). Since lighter rain is associated with weaker and lower diabatic heating, this bias in diabatic heating can be directly attributed to the lack of intense precipitation in the ORIG simulation. Weaker upper-level heating also inhibits the expected amplification of low-level convergence into the SPCZ, which is found in NEW and ERA5 but largely absent in ORIG. Stronger low-level convergence also derives in part from sharper local temperature gradients in NEW, which in turn result from a more realistic representation of shallow convective heating in the SPCZ region. Replacing the convection scheme also alters the climatological mean background state, with a narrower westerly duct over the eastern tropical Pacific in NEW relative to ORIG. This narrower westerly duct is consistent with the NEW simulation producing fewer, stronger convective events in the SPCZ, as suggested by van der Wiel et al. (2016a).

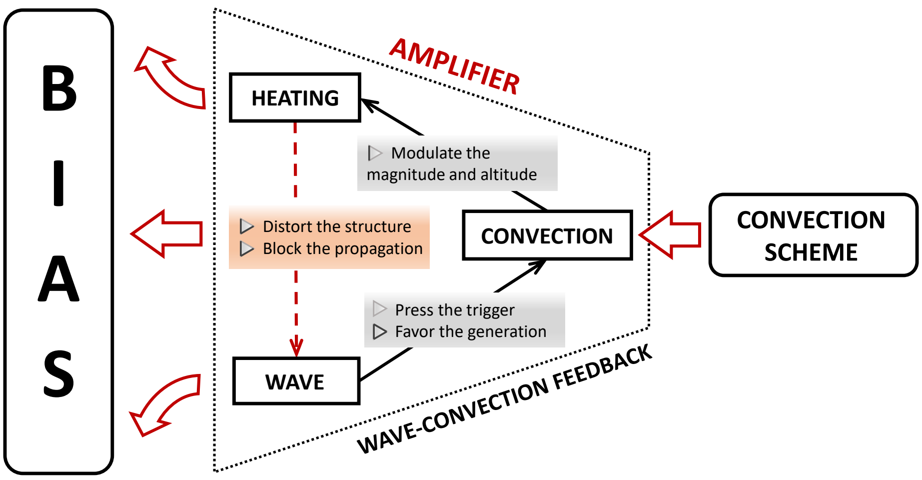

Figure 13. Schematic illustration of the mechanism underlying the impact of parameterized convection on the simulated SPCZ. The wave–convection feedback acts as an amplifier of the intrinsic bias in the original convective parameterization (red colored). An inability to produce enough intense precipitation (red arrow) reduces the impact of convective heating on the upper-level circulation (red dotted arrow), weakening the feedback and resulting in an even larger negative bias in intense precipitation.

The mechanism by which parameterized convection influences the SPCZ in our simulations is summarized in Figure 13. Transient Rossby waves passing through the SPCZ area play a critical role in SPCZ dynamics by triggering convection locally. The convection scheme used in the ORIG simulation produces a profile of diabatic heating during this convection that is both too weak in magnitude and too low in altitude, a bias that is largely eliminated in the NEW simulation. The stronger, higher diabatic heating in the NEW simulation distorts the transient wave, amplifying the downstream signal and opposing the upstream signal, and therefore blocking the wave from propagating continuously through the region (dashed red arrow in Figure 13). The secondary circulation produced by this wave–convection feedback further amplifies local convection, and therefore represents a positive feedback. The weaker, lower heating in the ORIG simulation fails to fully activate the distortion and blocking effects, weakening the secondary circulation and the associated positive feedback. Wave–convection feedbacks in the SPCZ therefore act to amplify the bias in the original convective parameterization. When these feedbacks are too weak, the SPCZ cannot maintain its subtropical branch, ultimately resulting in a weaker, more equatorward convergence zone and contributing to the double-ITCZ bias common to many GCMs.

While the simulations presented in this study demonstrate that parameterized convection influences the simulated SPCZ through the vertical distribution of latent heat release, it remains unclear which part or parts of the parameterization dominate this influence. Previous studies on the lack of intense precipitation in models using the ZM scheme have suggested that the small cloud base mass flux, which tightens the closure of the convection scheme, maybe the crucial factor. A small cloud base mass flux limits upward moisture transport, presenting a steeper barrier to strong deep convection and weakening the wave-convection feedback. Indeed, adding the stochastic scheme developed by Plant and Craig (2008) into the ZM scheme, which allows the generation of larger cloud base mass fluxes, has also been shown to improve the simulated SPCZ during austral summer (Wang et al., 2016). The cloud base mass flux in a single-column model using the NEW scheme is nearly twice that in the ZM scheme (Chu & Lin, 2023), lending further weight to this idea.

Open Research Section

Documentation, code, and example simulations based on CAM5 are available at https://www2.cesm.ucar.edu/models/cesm1.0/cam. Code and monthly outputs for runs based on the new convection scheme are available at https://doi.org/10.6084/m9.figshare.19474415.v1. This work has used daily ERA5 products on pressure levels (Hersbach, Bell, Berrisford, Biavati, et al., 2017a), single levels (Hersbach, Bell, Berrisford, Biavati, et al., 2017b), and model levels (Hersbach, Bell, Berrisford, Hirahara, et al., 2017) from the collections hosted by the Copernicus Climate Data Store (https://cds.climate.copernicus.eu), as well as IMERG data (GSFC, 2023) from the collection hosted by the National Aeronautics and Space Administration.

Acknowledgments

This work has been supported by the National Natural Science Foundation of China (grant numbers 41921005 and 42275053) and the Beijing Natural Science Foundation (grant number IS23121). We thank the European Centre for Medium-Range Weather Forecasts for producing the ERA5 reanalyses and providing access to these products.

References

Ashfaq, M., Skinner, C. B., & Diffenbaugh, N. S. (2010, July). Influence of sst biases on future climate change projections. *Climate Dynamics*, *36*(7–8), 1303–1319. Retrieved from `http://dx.doi.org/10.1007/s00382-010-0875-2` doi: 10.1007/s00382-010-0875-2

Bechtold, P., Köhler, M., Jung, T., Doblas-Reyes, F., Leutbecher, M., Rodwell, M. J., ... Balsamo, G. (2008, July). Advances in simulating atmospheric variability with the ecmwf model: From synoptic to decadal time-scales. *Quarterly Journal of the Royal Meteorological Society*, *134*(634), 1337–1351. Retrieved from `http://dx.doi.org/10.1002/qj.289` doi: 10.1002/qj.289

Beischer, T. A., Gregory, P., Dayal, K., Brown, J. R., Charles, A. N., Wang, W. X. D., & Brown, J. N. (2021, January). Scope for predicting seasonal variation of the spcz with access-s1. *Climate Dynamics*, *56*(5–6), 1519–1540. Retrieved from `http://dx.doi.org/10.1007/s00382-020-05550-6` doi: 10.1007/s00382-020-05550-6

Borlace, S., Santoso, A., Cai, W., & Collins, M. (2014, July). Extreme swings of the south pacific convergence zone and the different types of el niño events. *Geophysical Research Letters*, *41*(13), 4695–4703. Retrieved from `http://dx.doi.org/10.1002/2014GL060551` doi: 10.1002/2014gl060551

Brown, J. R., Lengaigne, M., Lintner, B. R., Widlansky, M. J., van der Wiel, K., Dutheil, C., ... Renwick, J. (2020). South Pacific Convergence Zone dynamics, variability and impacts in a changing climate. *Nature Reviews Earth & Environment*, *1*(10), 530–543. doi: 10.1038/s43017-020-0078-2

Brown, J. R., Moise, A. F., & Colman, R. A. (2012, November). The south pacific convergence zone in cmip5 simulations of historical and future climate. *Climate Dynamics*, *41*(7–8), 2179–2197. Retrieved from `http://dx.doi.org/10.1007/`

s00382-012-1591-x doi: 10.1007/s00382-012-1591-x

Brown, J. R., Power, S. B., Delage, F. P., Colman, R. A., Moise, A. F., & Murphy, B. F. (2011, March). Evaluation of the south pacific convergence zone in ipcc ar4 climate model simulations of the twentieth century. *Journal of Climate*, *24*(6), 1565–1582. Retrieved from http://dx.doi.org/10.1175/2010JCLI3942.1 doi: 10.1175/2010jcli3942.1

Cai, Q., Zhang, G. J., & Zhou, T. (2013). Impacts of shallow convection on MJO simulation: A moist static energy and moisture budget analysis. *Journal of Climate*, *26*(8), 2417–2431.

Cai, W., Lengaigne, M., Borlace, S., Collins, M., Cowan, T., McPhaden, M. J., … Widlansky, M. J. (2012). More extreme swings of the South Pacific convergence zone due to greenhouse warming. *Nature*, *488*, 365–369. doi: 10.1038/nature11358

Chang, E. K. M. (1993, July). Downstream development of baroclinic waves as inferred from regression analysis. *Journal of the Atmospheric Sciences*, *50*(13), 2038–2053. Retrieved from http://dx.doi.org/10.1175/1520-0469(1993)050<2038:ddobwa>2.0.co;2 doi: 10.1175/1520-0469(1993)050⟨2038:ddobwa⟩2.0.co;2

Chu, W., & Lin, Y. (2023, January). Description and evaluation of a new deep convective cloud model considering in-cloud inhomogeneity. *Journal of Advances in Modeling Earth Systems*, *15*(2). Retrieved from http://dx.doi.org/10.1029/2022ms003119 doi: 10.1029/2022ms003119

Dai, A. (2006, September). Precipitation characteristics in eighteen coupled climate models. *Journal of Climate*, *19*(18), 4605–4630. Retrieved from http://dx.doi.org/10.1175/JCLI3884.1 doi: 10.1175/jcli3884.1

De Almeida, R. A. F., Nobre, P., Haarsma, R. J., & Campos, E. J. D. (2007). Negative ocean-atmosphere feedback in the South Atlantic Convergence Zone. *Geophysical Research Letters*, *34*(18). doi: 10.1029/2007GL030401

Del Genio, A. D., Chen, Y., Kim, D., & Yao, M.-S. (2012). The mjo transition from shallow to deep convection in cloudsat/calipso data and giss gcm simulations. *Journal of Climate*, *25*(11), 3755–3770.

Grams, C. M., Wernli, H., Böttcher, M., Čampa, J., Corsmeier, U., Jones, S. C., … Wiegand, L. (2011, August). The key role of diabatic processes in modifying the upper-tropospheric wave guide: a north atlantic case-study. *Quarterly Journal of the Royal Meteorological Society*, *137*(661), 2174–2193. Retrieved from http://dx.doi.org/10.1002/qj.891 doi: 10.1002/qj.891

GSFC, P. P. S. P. A. N. (2023). *Gpm imerg final precipitation l3 half hourly 0.1 degree x 0.1 degree v07.* NASA Goddard Earth Sciences Data and Information Services Center. Retrieved from https://disc.gsfc.nasa.gov/datacollection/GPM_3IMERGHH_07.html doi: 10.5067/GPM/IMERG/3B-HH/07

Hagos, S., Zhang, C., Tao, W.-K., Lang, S., Takayabu, Y. N., Shige, S., … L'Ecuyer, T. (2010, February). Estimates of tropical diabatic heating profiles: Commonalities and uncertainties. *Journal of Climate*, *23*(3), 542–558. Retrieved from http://dx.doi.org/10.1175/2009jcli3025.1 doi: 10.1175/2009jcli3025.1

Hersbach, H., Bell, B., Berrisford, P., Biavati, G., Horányi, A., Muñoz Sabater, J., … Thépaut, J.-N. (2017a). *ERA5 monthly data on pressure levels from 1940 to present.* Copernicus Climate Change Service (C3S) Climate Data Store (CDS). doi: 10.24381/cds.6860a573

Hersbach, H., Bell, B., Berrisford, P., Biavati, G., Horányi, A., Muñoz Sabater, J., … Thépaut, J.-N. (2017b). *ERA5 monthly data on single levels from 1940 to present.* Copernicus Climate Change Service (C3S) Climate Data Store (CDS). doi: 10.24381/cds.f17050d7

Hersbach, H., Bell, B., Berrisford, P., Hirahara, S., Horányi, A., Muñoz-Sabater, J.,

... Thépaut, J.-N. (2020). The era5 global reanalysis. *Quarterly Journal of the Royal Meteorological Society*, *146*(730), 1999–2049. doi: 10.1002/qj.3803

Hersbach, H., Bell, B., Berrisford, P., Hirahara, S., Horányi, A., Muñoz-Sabater, J., ... Thépaut, J.-N. (2017). *Complete ERA5 from 1940: Fifth generation of ECMWF atmospheric reanalyses of the global climate.* Copernicus Climate Change Service (C3S) Data Store (CDS). doi: 10.24381/cds.143582cf

Hirota, N., Takayabu, Y. N., Watanabe, M., & Kimoto, M. (2011, September). Precipitation reproducibility over tropical oceans and its relationship to the double itcz problem in cmip3 and miroc5 climate models. *Journal of Climate*, *24*(18), 4859–4873. Retrieved from `http://dx.doi.org/10.1175/2011JCLI4156.1` doi: 10.1175/2011jcli4156.1

Hoskins, B. J., & Ambrizzi, T. (1993, June). Rossby wave propagation on a realistic longitudinally varying flow. *Journal of the Atmospheric Sciences*, *50*(12), 1661–1671. Retrieved from `http://dx.doi.org/10.1175/1520-0469(1993)050<1661:RWPOAR>2.0.CO;2` doi: 10.1175/1520-0469(1993)050⟨1661:rwpoar⟩2.0.co;2

Hoskins, B. J., McIntyre, M. E., & Robertson, A. W. (1985, October). On the use and significance of isentropic potential vorticity maps. *Quarterly Journal of the Royal Meteorological Society*, *111*(470), 877–946. Retrieved from `http://dx.doi.org/10.1002/qj.49711147002` doi: 10.1002/qj.49711147002

Hubert, L. F. (1961, March). A subtropical convergence line of the south pacific: A case study using meteorological satellite data. *Journal of Geophysical Research*, *66*(3), 797–812. Retrieved from `http://dx.doi.org/10.1029/JZ066i003p00797` doi: 10.1029/jz066i003p00797

Hurrell, J. W., Holland, M. M., Gent, P. R., Ghan, S., Kay, J. E., Kushner, P. J., ... others (2013). The Community Earth System Model: a framework for collaborative research. *Bulletin of the American Meteorological Society*, *94*(9), 1339–1360.

Kiladis, G. N., & Weickmann, K. M. (1992, September). Extratropical forcing of tropical pacific convection during northern winter. *Monthly Weather Review*, *120*(9), 1924–1939. Retrieved from `http://dx.doi.org/10.1175/1520-0493(1992)120<1924:EFOTPC>2.0.CO;2` doi: 10.1175/1520-0493(1992)120⟨1924:efotpc⟩2.0.co;2

Kun, L., Yimin, L., & Guoxiong, W. (2010). The impacts of the modified tiedtke cumulus convective parameterization scheme on the tropical rainfall simulation in samil model. *Chinese Journal of Atmospheric Sciences (in Chinese)*, *34*(1), 163–174. Retrieved from `http://www.dqkxqk.ac.cn/dqkx/dqkx/article/abstract/20100115` doi: 10.3878/j.issn.1006-9895.2010.01.15

Li, G., & Xie, S.-P. (2014, February). Tropical biases in cmip5 multimodel ensemble: The excessive equatorial pacific cold tongue and double itcz problems*. *Journal of Climate*, *27*(4), 1765–1780. Retrieved from `http://dx.doi.org/10.1175/jcli-d-13-00337.1` doi: 10.1175/jcli-d-13-00337.1

Li, L., Wang, B., Yuqing, W., & Hui, W. (2007, March). Improvements in climate simulation with modifications to the tiedtke convective parameterization in the grid-point atmospheric model of iap lasg (gamil). *Advances in Atmospheric Sciences*, *24*(2), 323–335. Retrieved from `http://dx.doi.org/10.1007/s00376-007-0323-3` doi: 10.1007/s00376-007-0323-3

Lin, J.-L. (2007, September). The double-itcz problem in ipcc ar4 coupled gcms: Ocean–atmosphere feedback analysis. *Journal of Climate*, *20*(18), 4497–4525. Retrieved from `http://dx.doi.org/10.1175/JCLI4272.1` doi: 10.1175/jcli4272.1

Lin, J.-L., Kiladis, G. N., Mapes, B. E., Weickmann, K. M., Sperber, K. R., Lin, W., ... Scinocca, J. F. (2006, June). Tropical intraseasonal variability in 14 ipcc ar4 climate models. part i: Convective signals. *Journal of Climate*, *19*(12), 2665–2690. Retrieved from `http://dx.doi.org/10.1175/JCLI3735.1` doi:

10.1175/jcli3735.1

Lin, Y., Zhao, M., Ming, Y., Golaz, J.-C., Donner, L. J., Klein, S. A., … Xie, S. (2013, July). Precipitation partitioning, tropical clouds, and intraseasonal variability in gfdl am2. *Journal of Climate*, *26*(15), 5453–5466. Retrieved from `http://dx.doi.org/10.1175/jcli-d-12-00442.1` doi: 10.1175/jcli-d-12-00442.1

Lin, Z. (2019). The South Atlantic–South Indian Ocean pattern: a zonally oriented teleconnection along the Southern Hemisphere westerly jet in Austral summer. *Atmosphere*, *10*(5), 259. doi: 10.3390/atmos10050259

Lintner, B. R., Langenbrunner, B., Neelin, J. D., Anderson, B. T., Niznik, M., Li, G., & Xie, S. (2016, October). Characterizing cmip5 model spread in simulated rainfall in the pacific intertropical convergence and south pacific convergence zones. *Journal of Geophysical Research: Atmospheres*, *121*(19), 11590–11607. Retrieved from `http://dx.doi.org/10.1002/2016JD025284` doi: 10.1002/2016jd025284

Lintner, B. R., & Neelin, J. D. (2008, August). Eastern margin variability of the south pacific convergence zone. *Geophysical Research Letters*, *35*(16). Retrieved from `http://dx.doi.org/10.1029/2008GL034298` doi: 10.1029/2008gl034298

Matthews, A. J. (2012). A multiscale framework for the origin and variability of the South Pacific Convergence Zone. *Quarterly Journal of the Royal Meteorological Society*, *138*(666), 1165–1178. doi: 10.1002/qj.1870

Matthews, A. J., Hoskins, B. J., Slingo, J. M., & Blackburn, M. (1996, April). Development of convection along the spcz within a madden-julian oscillation. *Quarterly Journal of the Royal Meteorological Society*, *122*(531), 669–688. Retrieved from `http://dx.doi.org/10.1002/qj.49712253106` doi: 10.1002/qj.49712253106

Mechoso, C., Robertson, A., Barth, N., Davey, M., Delecluse, P., Gent, P., … Tribbia, J. (1995, September). The seasonal cycle over the tropical pacific in coupled ocean–atmosphere general circulation models. *Monthly Weather Review*, *123*(9), 2825–2838. Retrieved from `http://dx.doi.org/10.1175/1520-0493(1995)123<2825:TSCOTT>2.0.CO;2` doi: 10.1175/1520-0493(1995)123⟨2825:tscott⟩2.0.co;2

Morrison, H., & Gettelman, A. (2008, August). A new two-moment bulk stratiform cloud microphysics scheme in the community atmosphere model, version 3 (cam3). part i: Description and numerical tests. *Journal of Climate*, *21*(15), 3642–3659. Retrieved from `http://dx.doi.org/10.1175/2008JCLI2105.1` doi: 10.1175/2008jcli2105.1

Neale, R. B., Chen, C.-C., Gettelman, A., Lauritzen, P. H., Park, S., Williamson, D. L., … others (2010). Description of the ncar community atmosphere model (cam 5.0). *NCAR Tech. Note NCAR/TN-486+ STR*, *1*(1), 1–12.

Neale, R. B., Richter, J. H., & Jochum, M. (2008, November). The impact of convection on enso: From a delayed oscillator to a series of events. *Journal of Climate*, *21*(22), 5904–5924. Retrieved from `http://dx.doi.org/10.1175/2008jcli2244.1` doi: 10.1175/2008jcli2244.1

Niznik, M. J., & Lintner, B. R. (2013). Circulation, moisture, and precipitation relationships along the south pacific convergence zone in reanalyses and cmip5 models. *Journal of Climate*, *26*(24), 10174–10192. Retrieved from `http://dx.doi.org/10.1175/jcli-d-13-00263.1` doi: 10.1175/jcli-d-13-00263.1

Niznik, M. J., Lintner, B. R., Matthews, A. J., & Widlansky, M. J. (2015). The role of tropical–extratropical interaction and synoptic variability in maintaining the south pacific convergence zone in cmip5 models. *Journal of Climate*, *28*(8), 3353–3374. Retrieved from `http://dx.doi.org/10.1175/jcli-d-14-00527.1` doi: 10.1175/jcli-d-14-00527.1

Oueslati, B., & Bellon, G. (2013, April). Convective entrainment and large-scale organization of tropical precipitation: Sensitivity of the cnrm-cm5 hierarchy of models. *Journal of Climate*, *26*(9), 2931–2946. Retrieved from `http://dx.doi.org/10.1175/JCLI-D-12-00314.1` doi: 10.1175/jcli-d-12-00314.1

Park, S. (2014, October). A unified convection scheme (unicon). part i: Formulation. *Journal of the Atmospheric Sciences*, *71*(11), 3902–3930. Retrieved from `http://dx.doi.org/10.1175/JAS-D-13-0233.1` doi: 10.1175/jas-d-13-0233.1

Plant, R. S., & Craig, G. C. (2008, January). A stochastic parameterization for deep convection based on equilibrium statistics. *Journal of the Atmospheric Sciences*, *65*(1), 87–105. Retrieved from `http://dx.doi.org/10.1175/2007JAS2263.1` doi: 10.1175/2007jas2263.1

Senapati, B., Deb, P., Dash, M. K., & Behera, S. K. (2022). Origin and dynamics of global atmospheric wavenumber-4 in the Southern mid-latitude during austral summer. *Climate Dynamics*, *59*(5-6), 1309–1322. doi: 10.1007/s00382-021-06040-z

Song, X., & Zhang, G. J. (2018, March). The roles of convection parameterization in the formation of double itcz syndrome in the ncar cesm: I. atmospheric processes. *Journal of Advances in Modeling Earth Systems*, *10*(3), 842–866. Retrieved from `http://dx.doi.org/10.1002/2017MS001191` doi: 10.1002/2017ms001191

Takahashi, K., & Battisti, D. S. (2007, December). Processes controlling the mean tropical pacific precipitation pattern. part ii: The spcz and the southeast pacific dry zone. *Journal of Climate*, *20*(23), 5696–5706. Retrieved from `http://dx.doi.org/10.1175/2007JCLI1656.1` doi: 10.1175/2007jcli1656.1

Taylor, K. E., Stouffer, R. J., & Meehl, G. A. (2012, April). An overview of cmip5 and the experiment design. *Bulletin of the American Meteorological Society*, *93*(4), 485–498. Retrieved from `http://dx.doi.org/10.1175/BAMS-D-11-00094.1` doi: 10.1175/bams-d-11-00094.1

Trenberth, K. E. (1976). Spatial and temporal variations of the southern oscillation. *Quarterly Journal of the Royal Meteorological Society*, *102*(433), 639–653. Retrieved from `http://dx.doi.org/10.1002/qj.49710243310` doi: 10.1002/qj.49710243310

van der Wiel, K., Matthews, A. J., Joshi, M. M., & Stevens, D. P. (2016a). The influence of diabatic heating in the South Pacific Convergence Zone on Rossby wave propagation and the mean flow. *Quarterly Journal of the Royal Meteorological Society*, *142*(695), 901–910. doi: https://doi.org/10.1002/qj.2692

van der Wiel, K., Matthews, A. J., Joshi, M. M., & Stevens, D. P. (2016b). Why the South Pacific Convergence Zone is diagonal. *Climate Dynamics*, *46*(5-6), 1683–1698. doi: 10.1007/s00382-015-2668-0

van der Wiel, K., Matthews, A. J., Stevens, D. P., & Joshi, M. M. (2015). A dynamical framework for the origin of the diagonal South Pacific and South Atlantic Convergence Zones. *Quarterly Journal of the Royal Meteorological Society*, *141*(691), 1997–2010. doi: 10.1002/qj.2508

Vincent, D. G. (1994). The South Pacific Convergence Zone (SPCZ): A review. *Monthly Weather Review*, *122*(9), 1949–1970. doi: 10.1175/1520-0493(1994)122⟨1949:tspcza⟩2.0.co;2

Vincent, E. M., Lengaigne, M., Menkes, C. E., Jourdain, N. C., Marchesiello, P., & Madec, G. (2011). Interannual variability of the South Pacific Convergence Zone and implications for tropical cyclone genesis. *Climate Dynamics*, *36*(9-10), 1881–1896. Retrieved from `http://dx.doi.org/10.1007/s00382-009-0716-3` doi: 10.1007/s00382-009-0716-3

Wang, Y., Zhang, G. J., & Craig, G. C. (2016). Stochastic convective parameterization improving the simulation of tropical precipitation variability in the NCAR CAM5. *Geophysical Research Letters*, *43*(12), 6612–6619. doi:

10.1002/2016gl069818

Widlansky, M. J., Webster, P. J., & Hoyos, C. D. (2010, July). On the location and orientation of the south pacific convergence zone. *Climate Dynamics*, *36*(3–4), 561–578. Retrieved from `http://dx.doi.org/10.1007/s00382-010-0871-6` doi: 10.1007/s00382-010-0871-6

Wright, J. S., Fu, R., Worden, J. R., Chakraborty, S., Clinton, N. E., Risi, C., … Yin, L. (2017, July). Rainforest-initiated wet season onset over the southern amazon. *Proceedings of the National Academy of Sciences*, *114*(32), 8481–8486. Retrieved from `http://dx.doi.org/10.1073/pnas.1621516114` doi: 10.1073/pnas.1621516114

Yanai, M., Esbensen, S., & Chu, J.-H. (1973, May). Determination of bulk properties of tropical cloud clusters from large-scale heat and moisture budgets. *Journal of the Atmospheric Sciences*, *30*(4), 611–627. Retrieved from `http://dx.doi.org/10.1175/1520-0469(1973)030<0611:DOBPOT>2.0.CO;2` doi: 10.1175/1520-0469(1973)030⟨0611:dobpot⟩2.0.co;2

Zhang, G., & McFarlane, N. A. (1995). Sensitivity of climate simulations to the parameterization of cumulus convection in the Canadian climate centre general circulation model. *Atmosphere-Ocean*, *33*(3), 407–446. (the original ZM paper) doi: 10.1080/07055900.1995.9649539

Zhang, G. J., & Mu, M. (2005, May). Effects of modifications to the zhang-mcfarlane convection parameterization on the simulation of the tropical precipitation in the national center for atmospheric research community climate model, version 3. *Journal of Geophysical Research: Atmospheres*, *110*(D9). Retrieved from `http://dx.doi.org/10.1029/2004JD005617` doi: 10.1029/2004jd005617

Zhang, G. J., & Song, X. (2010, February). Convection parameterization, tropical pacific double itcz, and upper-ocean biases in the ncar ccsm3. part ii: Coupled feedback and the role of ocean heat transport. *Journal of Climate*, *23*(3), 800–812. Retrieved from `http://dx.doi.org/10.1175/2009jcli3109.1` doi: 10.1175/2009jcli3109.1

Zhang, G. J., & Wang, H. (2006, March). Toward mitigating the double itcz problem in ncar ccsm3. *Geophysical Research Letters*, *33*(6). Retrieved from `http://dx.doi.org/10.1029/2005gl025229` doi: 10.1029/2005gl025229

Zhang, X., Liu, H., & Zhang, M. (2015, October). Double itcz in coupled ocean-atmosphere models: From cmip3 to cmip5: Double itcz in cmip3 and cmip5 aogcms. *Geophysical Research Letters*, *42*(20), 8651–8659. Retrieved from `http://dx.doi.org/10.1002/2015gl065973` doi: 10.1002/2015gl065973